Dynamic Thermal Field-Induced Gradient Soft-Shear for Highly Oriented Block Copolymer Thin Films

Gurpreet Singh,[†] Kevin G. Yager,[‡] Brian Berry,[§] Ho-Cheol Kim,[⊥] and Alamgir Karim[†,*]

[†]Department of Polymer Engineering, The University of Akron, Akron, Ohio 44325, United States, [‡]Center for Functional Nanomaterials, Brookhaven National Laboratory, Upton, New York 11973, United States, [§]Department of Chemistry, University of Arkansas at Little Rock, Little Rock, Arkansas 72204, United States, and [⊥]IBM Research Division, Almaden Research Center, San Jose, California 95120-6099, United States

ABSTRACT As demand for smaller, more powerful, and energy-efficient devices continues, conventional patterning technologies are pushing up against fundamental limits. Block copolymers (BCPs) are considered prime candidates for a potential solution *via* directed self-assembly of nanostructures. We introduce here a facile directed self-assembly method to rapidly fabricate unidirectionally aligned BCP nanopatterns at large scale, on rigid or flexible template-free substrates *via* a thermally induced dynamic gradient soft-shear field. A localized differential thermal expansion at the interface between a BCP film and a confining polydimethylsiloxane (PDMS) layer due to a dynamic thermal field imposes the gradient soft-shear field. PDMS undergoes directional expansion (along the annealing direction) in the heating zone and contracts back in the cooling zone, thus setting up a single cycle of oscillatory shear (maximum lateral shear stress $\sim 12 \times 10^4$ Pa) in the system. We successfully apply this process to create unidirectional alignment of BCP thin films over a wide range of thicknesses (nm to μm) and processing speeds (μm/s to mm/s) using both a flat and patterned PDMS layer. Grazing incidence small-angle X-ray scattering measurements show absolutely no sign of isotropic population and reveal $\geq$99% aligned orientational order with an angular spread $\Delta\theta_{fwhm} \leq 5°$ (full width at half-maximum). This method may pave the way to practical industrial use of hierarchically patterned BCP nanostructures.

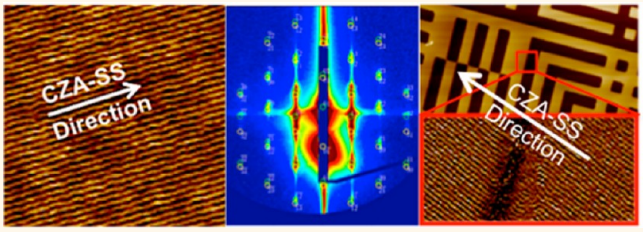

KEYWORDS: block copolymer · zone annealing · unidirectional nanostructures · thermal expansion induced shear · flexible substrate · PDMS template · hierarchical patterning

Directed self-assembly (DSA) of block copolymers (BCPs) has been proposed as an economical route to overcome the lithographic limitations set by the optical processes and the available photoresist materials.[1,2] BCP self-assembly has been mastered to a great extent,[3] and several techniques[4−10] exist to create precise arrays of desired nanostructures. Although prototype devices[11−17] demonstrate the usability of BCP nanostructures, their continuous mass production remains a persistent challenge. In most cases, mass production is bounded by the inability to scale-up the complex techniques used to direct the BCP self-assembly. Additionally, successful process scale-up demands not only excellent pattern quality but also rapid patterning over large areas. As highlighted by Buriak *et al.*,[18] the semiconductor industry typically requires patterning to be completed within 4 min. Keeping industrial scale-up in mind, zone annealing (ZA) or zone refining,[19] has recently been applied to direct self-assembly of BCP systems.[20−23] ZA is traditionally used for refining metals and semiconductor wafers, where the specimen passes through a temperature gradient that restricts the crystal growth to a narrow zone. Lovinger *et al.*[24] conducted pioneering studies on ZA of crystalline homopolymers, where they established the importance of temperature gradients, growth rate, and degree of superheat. Previous BCP−ZA efforts yielded mixed results. Millimeter-size grains were only achieved for bulk films that were annealed at extremely slow speeds (2 mm/day) when the maximum temperature (T_{MAX}) of the temperature gradient was above the BCP order−disorder transition temperature (T_{ODT}), thus making the process practically unfeasible and applicable only to the select few block copolymers with accessible T_{ODT} values.[20] It is worthy to mention that there

* Address correspondence to alamgir@uakron.edu.

Received for review September 15, 2012 and accepted October 24, 2012.

Published online October 24, 2012
10.1021/nn304266f

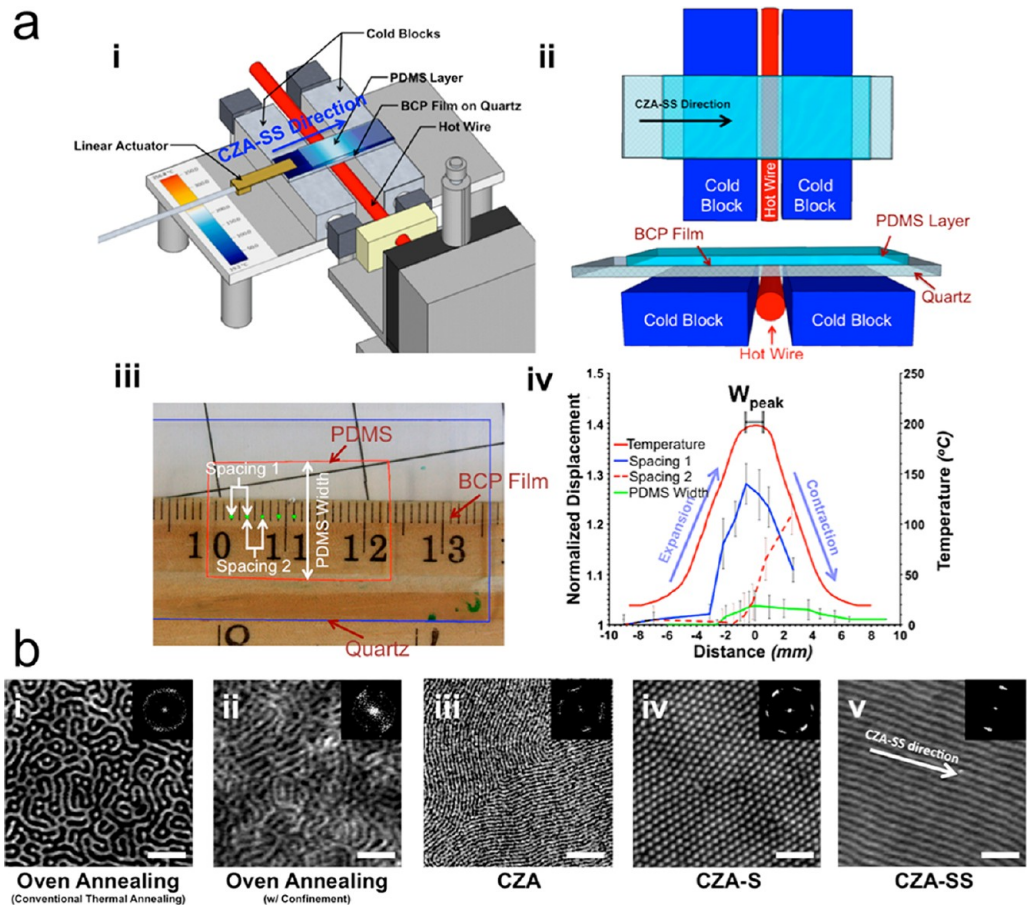

Figure 1. CZA−SS process dynamics and its effect on BCP morphology. (a) (i) Schematic of the CZA−SS apparatus. (ii) In-plane and out-of-plane view of the CZA−SS process. (iii) Model assembly of quartz−BCP−PDMS system. Fiduciary marks (spacing 1, spacing 2) on PDMS and PDMS width (*W*), as shown, enable expansion−contraction calculations. (iv) Temperature gradient curve is shown along with corresponding calculated normalized displacement of PDMS in the CZA−SS direction (spacing 1, spacing 2; refer to panel a,iii) and orthogonal (PDMS width; refer to panel a,iii) to it. (b) AFM images of 700 nm thick PS-PMMA (82 kg/mol) films after (i) thermal annealing in a conventional vacuum oven at 200 °C for 24 h; (ii) thermal annealing in a conventional vacuum oven under PDMS confinement at 200 °C for 24 h; (iii) 47.5 kg/mol PS-PMMA, CZA annealed at $\nabla T \sim 24$ °C mm^{-1}, $T_{MAX} \sim 220$ °C mm^{-1}, and $V = 5$ μm/s; (iv) CZA−sharp thermal gradient (CZA-S) at $\nabla T \sim 45$ °C mm^{-1}, $T_{MAX} \sim 210$ °C mm^{-1}, and $V = 5$ μm/s; (v) CZA−SS annealed at $\nabla T \sim 45$ °C mm^{-1}, $T_{MAX} \sim 200$ °C mm^{-1}, and $V = 5$ μm/s. Insets show corresponding FFTs. Size of scale bar is 200 nm.

are a few other reports[25] of roll-to-roll processes for DSA of BCPs; however, these methods are highly specific to liquid crystal BCPs. A modified, more practical version of ZA, termed cold zone annealing (CZA)[22] where $T_{MAX} \ll T_{ODT}$, demonstrated that, for the BCP cylinder phase, shallow thermal gradients lead to horizontal cylinders with long-range order, faster ordering kinetics compared to conventional oven annealing, and orientational control albeit with many defects. Recently pioneered techniques, namely, mechanical soft-shear alignment[26−28] and faceted substrates,[29,30] have been documented to produce oriented horizontal BCP cylinders on macroscopic scales. Faceted or templated substrate adds an additional processing step where as it is argued[29] that mechanical soft-shear alignment is limited by BCP film thickness.

Here, we demonstrate the ability to controllably fabricate highly oriented horizontal BCP cylinders on physical or chemical template-free substrates that may be rigid or flexible, *via* a novel dynamic thermal field-induced gradient soft-shear process that we refer to as CZA−soft-shear or "CZA−SS". Using CZA−SS, arrays of hexagonally packed and horizontally aligned BCP cylinders in films over a thickness range, $40 \leq h \leq 1000$ nm, with greater than 99% cylinder alignment in CZA−SS direction, with $\Delta\theta_{fwhm} < 5°$ (full width at half-maximum angular spread), can be fabricated at relatively high velocities for BCP ordering ($V \approx 0.2$ mm/s, *i.e.*, 12 mm/min) over unlimited dimensions. The CZA−SS method is applicable to any BCP with an accessible glass transition temperature (T_g) as the $T_{MAX} \ll T_{ODT}$.

RESULTS AND DISCUSSION

A schematic of the CZA−SS setup is shown in Figure 1a(i). The horizontal temperature gradient apparatus is the same as that used in our previous study.[23] The quartz-coated cylindrical poly(styrene-*block*-methylmethacrylate) (PS-PMMA) BCP film is then conformally

covered with a cross-linked polydimethylsiloxane (PDMS) layer with a thickness of 0.3 ± 0.1 mm with the same lateral dimensions as the BCP film. A PDMS roller could alternatively be used for continuous roll-to-roll (R2R) manufacturing. The PDMS-confined BCP film is then passed across the temperature gradient (∇T) with a predefined velocity. T_{MAX} and ∇T_{MAX} for the CZA−SS process were 200 and 45 °C/mm, respectively. After processing, the PDMS layer is cleanly peeled off, thus allowing characterization of the underlying BCP film. Figure 1a(ii) shows a schematic of the CZA−SS process dynamics. The coefficient of linear thermal expansion (CTE, α) of PDMS is ∼5 times that of PS-PMMA ($\alpha_{PDMS} = 325 \times 10^{-6}$/°C; $\alpha_{PS} = 80 \times 10^{-6}$/°C; $\alpha_{PMMA} = 50 \times 10^{-6}$/°C).[31] The lateral thermal expansion of the PS-PMMA at the substrate interface is restricted due to PMMA adhesion.[32] Likewise, the lateral thermal expansion of the top PDMS−BCP interface is restricted *via* glassy BCP behavior until reaching its T_g on the thermal gradient (*ca.* 115−120 °C from Figure 1a), at which point the PDMS overlayer starts to expand, inducing shear at the PDMS−BCP interface. PDMS overlayer exhibits excellent adhesion with the substrate-supported PS-PMMA film and does not delaminate at the reported processing conditions. We visualized the thermal expansion profile of the PDMS overlayer with fiduciary marks *via* digitized imagery along the length (*L*) and width (*W*) directions (Figure 1a(iii)). Figure 1a(iv) shows a normalized, local expansion to contraction shear behavior of PDMS as it crosses T_{MAX}. Normalized PDMS length changes occurring along CZA−SS direction are much larger than the normalized PDMS width changes orthogonal to the CZA−SS direction. This thermally induced directional and oscillatory local PDMS displacement shearing the underlying BCP film (assuming no-slip condition) is the fundamental ordering mechanism, yielding macroscopic unidirectionally aligned highly ordered BCP structures without the use of any template. Thermal expansion-induced shear stress (σ) is given by the equation $\sigma_{PDMS} = G_{PDMS} \times \gamma_{MAX}$, where γ_{MAX} is the maximum strain and G_{PDMS} is the shear modulus of PDMS (*ca.* 0.4 MPa).[33] The calculated $\gamma_{MAX} = 0.3$ from Figure 1a(iv) and corresponding $\sigma_{PDMS} = 12 \times 10^4$ Pa. The shear stresses generated in CZA−SS are a magnitude greater than reported for mechanical soft-shear alignment studies[26−28] of cylindrical BCP thin films. Notable differences in these methods include localized shear zone, gradient temperature profile, and single oscillation shear in CZA−SS *versus* the full-sample area, constant temperature, constant shear, and unidirectional shear in mechanical soft-shear studies. Figure 1b shows that the BCP cylinder morphology becomes highly aligned under this remarkable unidirectional ordering in CZA−SS. The thermal gradient plays a significant role in the unidirectional alignment and grain growth by lowering the activation energy required for cylinder reorientation process.[34] Figure 1b compares the CZA−SS process with uniform thermal oven annealing and previous[22,23] CZA modes.

A key feature of the CZA−SS technique is the ability to align BCP films over a wide thickness range. We confirm aligned films ranging in thickness that form a monolayer of cylinders, $h = 40$ nm (BCP domain spacing ∼24 nm), up to 44 layers of hexagonally packed horizontal cylinders at $h = 1000$ nm, at speeds ranging from $V = 1$ μm/s (or 60 μm/min) up to industrially relevant speeds of $V = 12$ mm/min (Figure 2). Previous studies on horizontal alignment of cylinders in the thin film regime have focused on monolayer film thicknesses. Register *et al.*[26] found that morphological defects increased exponentially when the film thickness was greater or less than the exact monolayer thickness. Russell *et al.*[29] surpassed this monolayer thickness limit *via* faceted substrates, obtaining unidirectional horizontal cylinders for films less than 2 domains thick. In this study, we extend this aligned thickness limit by more than an order of magnitude, up to 44 layers (∼1 μm) (Figure 2), and atomic force microscopy (AFM) shows fully aligned films even up to 1.5 μm, but their internal structure was not characterized. Excitingly, Figure 2 also shows that CZA−SS can fabricate highly aligned BCP patterns of 2 cm length over arbitrary width in less than 1 min, approximately 2 orders of magnitude faster than annealing times reported in previous studies using mechanical soft-shear alignment[26,28] and faceted substrates[29] for similar ordered dimensions. Orientation analysis for a 4×40 μm^2 composite AFM image (see Supporting Information Figure S1) of a CZA−SS annealed PS-PMMA thin film reveals a single grain (*i.e.*, a single crystal), with $\Delta\theta_{fwhm} \sim 5°$ and 95% preservation of orientation order over arbitrary distances. Such rapid formation of unidirectionally aligned BCP single crystals over unlimited dimensions is a major advancement over what is achievable with conventional oven annealing.

Grazing incidence small-angle X-ray scattering (GISAXS) with varying azimuthal (in-plane) sample angle was performed to compare the AFM surface morphology with the through-film thickness orientation (Figure 3). GISAXS experiments were performed at incidence angles that were above the film−vacuum critical angle, thus ensuring that the X-rays penetrated and measured the entire film thickness. GISAXS confirms that, even for the thickest films studied (*ca.* 1000 nm), the uniaxial orientation imposed by CZA−SS is propagated throughout the entire film thickness. In fact, the orientational order is more robust in *thicker* films. Apparently, reduced polymer mobility near the hard substrate interface counteracts the shear-induced ordering phenomena in very thin films ($h < 40$ nm). Nevertheless, even for less than monolayer thickness films ($h <$ 24 nm), alignment is robust ($\Delta\theta_{fwhm} \approx 11°$), and in thick films ($h \geq 60$ nm), the entire film thickness is extremely well-aligned ($\Delta\theta_{fwhm} < 5°$). The numerous,

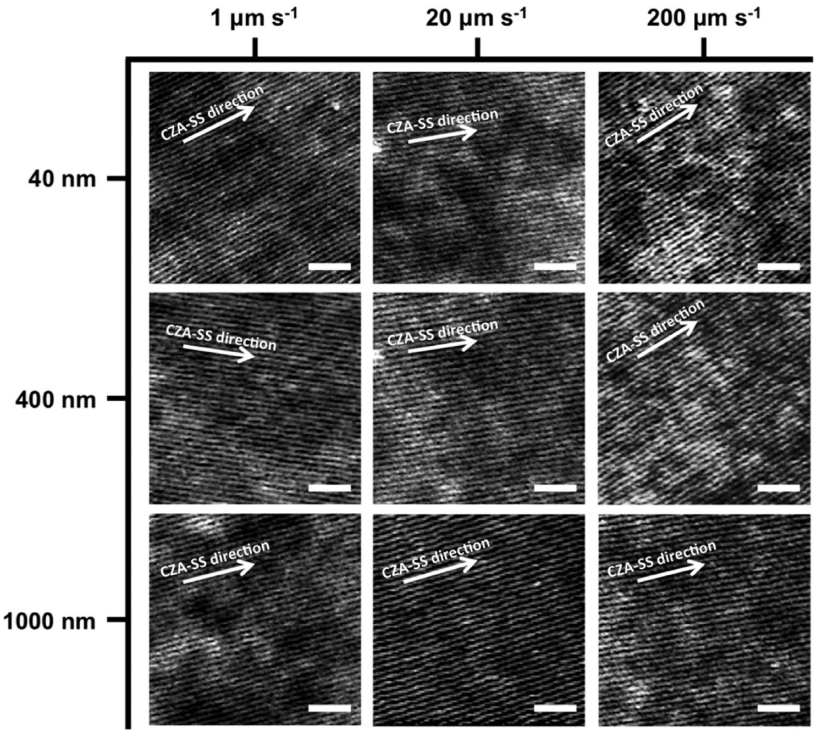

Figure 2. Influence of BCP film thickness and CZA−SS annealing velocity on BCP morphology. AFM images of PS-PMMA (47.5 kg/mol) films with varying film thickness and CZA−SS annealing velocity. Arrows show the CZA−SS direction. Size of scale bar is 200 nm.

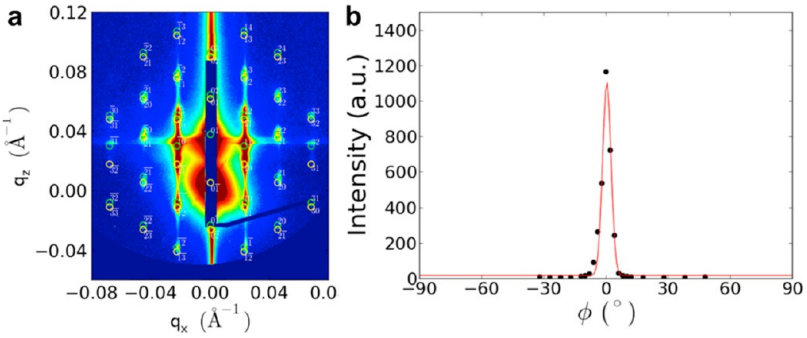

Figure 3. BCP orientation analysis *via* GISAXS. (a) Representative image of a BCP thin film, annealed and oriented using CZA−SS, measured using grazing incidence small-angle X-ray scattering (GISAXS). The sharp higher-order peaks result from large, well-defined grains. The peak positions can be explained by a hexagonal unit cell well-aligned with the substrate direction. There is no signature of an isotropic population or of vertically aligned cylinders within the film. (b) Azimuthal angle analysis. The background-corrected scattering intensity of the first-order peak is plotted as a function of the in-plane angle, ϕ. The peak width provides a measure of the grain alignment with respect to the direction of the CZA−SS processing.

sharp higher-order peaks in Figure 3 are a signature of the large, well-ordered grains spanning the entire film. The peak positions are indexed to a hexagonal unit cell that is highly aligned with the substrate direction. Additionally, there is absolutely no signature of isotropically or vertically aligned cylinders within the film. The patterns thus obtained *via* CZA−SS are fully aligned (near perfect) but exhibit minor short-range variations about the principle alignment axis. We believe that CZA−SS of a judicious choice of a BCP system with a very high interaction parameter and lower molecular weight, such as poly(styrene-*block*-polydimethylsiloxane) or poly(styrene-*block*-trimethylsilylisoprene),[35] may lead to perfect BCP patterns. Additionally, an overlayer with higher shear modulus and higher coefficient of thermal expansion should facilitate the fabrication of perfect BCP patterns. We are currently investigating these avenues.

The BCP orientation in CZA−SS is controlled by the induced shear direction that can be controlled by the confining PDMS overlayer geometry (shape and size) relative to the CZA−SS annealing direction. PDMS overlayer's of different symmetric and asymmetric dimensions were used to study the effect of the overlayer geometry on the BCP morphology (inset Figure 4). L_{PDMS} refers to the overlayer length along the direction of CZA−SS motion and W_{PDMS} to the overlayer width

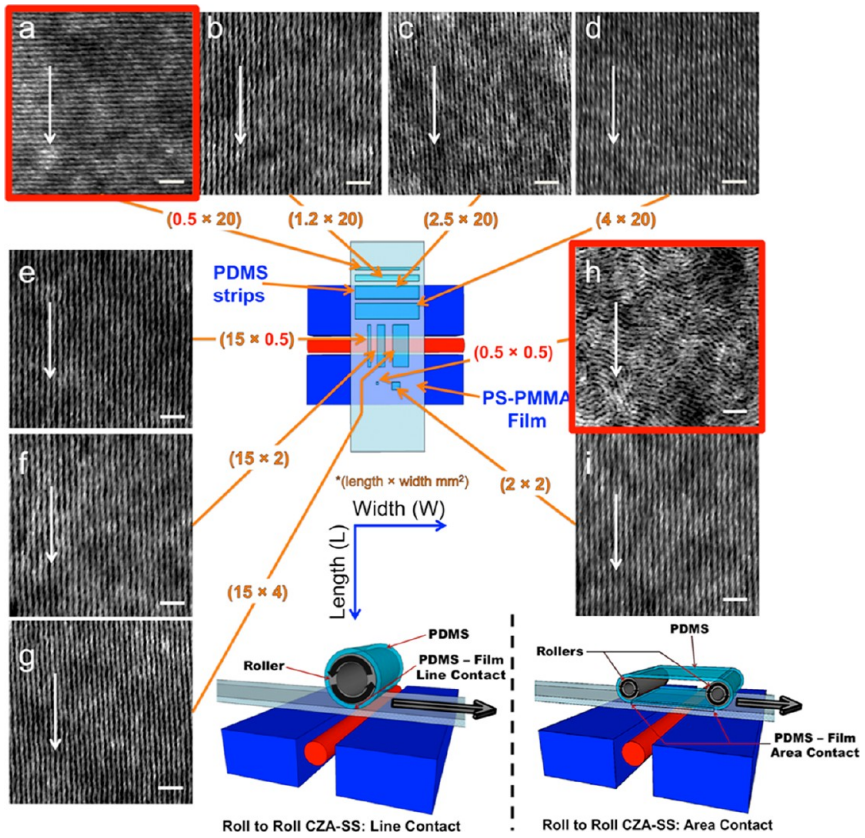

Figure 4. Influence of PDMS layer geometry and dimensions on BCP orientation. Schematic of the CZA−SS experiment utilizing different PDMS layer geometries and dimensions is shown as an inset. AFM images of the CZA−SS annealed BCP film with specific PDMS dimensions are shown. PDMS layer dimensions for corresponding images are (a) 0.5 mm × 20 mm, (b) 1.2 mm × 20 mm, (c) 2.5 mm × 20 mm, (d) 4 mm × 20 mm, (e) 15 mm × 0.5 mm, (f) 15 mm × 2 mm, (g) 15 mm × 4 mm, (h) 0.5 mm × 0.5 mm, and (i) 2 mm × 2 mm. Arrows show CZA−SS direction. Size of scale bar is 200 nm.

orthogonal to it. Figure 4b−d and Figure 4e−g show that horizontal PS-PMMA cylinders are aligned with the CZA−SS direction providing $L_{PDMS} > W_{peak}$ (≈1 mm), where W_{peak} is the dimension of the shallow gradient temperature region corresponding to roughly the hot-wire diameter (refer to Figure 1a(iv)). Under these conditions, the increasing lateral temperature gradient produces a greater strain (and therefore greater shear) along the CZA−SS direction compared to the orthogonal direction, so that BCP cylinders align in the CZA−SS direction. In contrast, Figure 4a shows that horizontal PS-PMMA cylinders are oriented *orthogonal* to the CZA−SS direction when $L_{PDMS} < W_{peak}$. This is caused by a larger relative expansion of the narrow ($W_{PDMS}/L_{PDMS} \sim 50$) PDMS strip orthogonal to the CZA−SS direction, due to a geometry-dominated highly asymmetric expansion over the W_{peak} zone. Clearly, PDMS layer asymmetry ratio is important, suggesting that a R2R assembly, with a 1 mm width top-contacting PDMS roller, will drive orthogonally aligned BCP cylinders.

Results reported so far were with asymmetric PDMS geometries (*i.e.*, rectangles with $L_{PDMS} \neq W_{PDMS}$). Large square (symmetric) patterns with $L_{PDMS} = W_{PDMS} > W_{peak}$ lead to horizontal cylinders aligned in the CZA−SS direction (Figure 4i), in accordance with previous results on asymmetric PDMS overlayers for the same reasons. In contrast, for a miniaturized square PDMS overlayer, with $L_{PDMS} = W_{PDMS} = W_{peak}$ (≈1 mm), the horizontal cylinders are oriented randomly (Figure 4h). This is due to a small relative physical expansion of PDMS due to its small dimension and placement over a shallow $\nabla T \approx 0$ °C/mm region.

Our observations have enumerated important CZA−SS parameters for high BCP alignment on quartz substrates, that is, a sharp ∇T and a BCP capping PDMS overlayer with controlled geometric shape, aspect ratio, and physical dimension relative to the hot-wire zone. CZA−SS is, in fact, a very general process applicable to other BCP systems and substrates. Currently, significant effort is being directed toward developing next-generation nanoelectronics on flexible substrates, but studies on ordering of BCP films on flexible substrates is relatively scant.[23,25,29,36] We observed that the CZA−SS process is eminently applicable to inducing alignment of cylindrical PS-PMMA films cast on flexible substrates as well as polyimide films "Kapton" (see Supporting Information Figure S2). Figure 5a shows AFM and GISAXS of highly oriented horizontal poly(styrene-*block*-2-vinylpyridine) (PS-P2VP) cylinders, CZA-SS processed similarly to cylindrical PS-PMMA. The sharp fourth-order

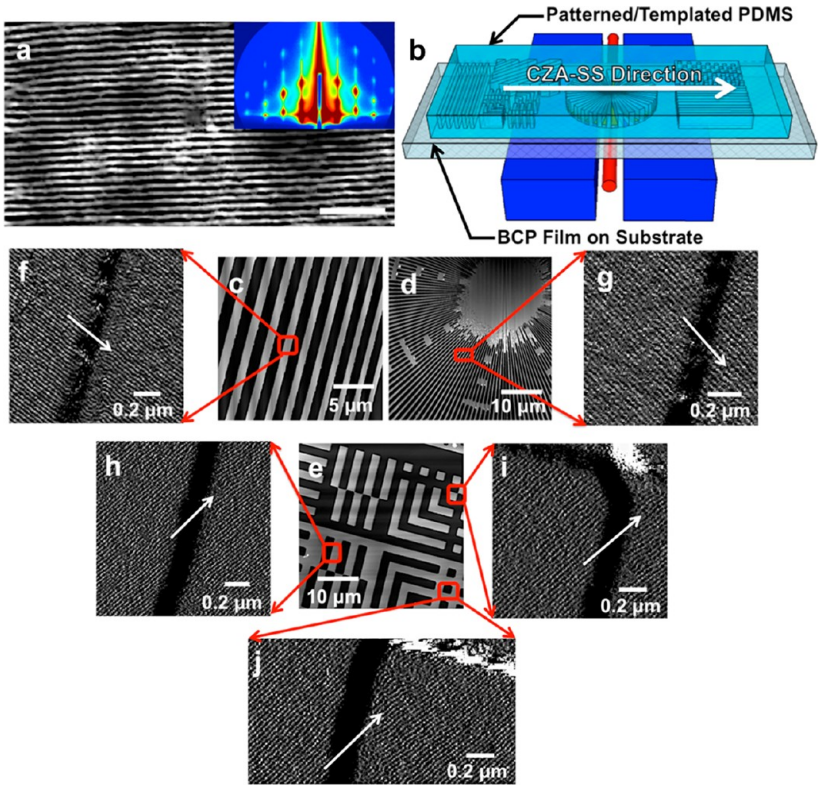

Figure 5. Robustness of the CZA−SS process. (a) AFM image of a 100 nm PS-P2VP (34 kg/mol) film that was CZA−SS annealed at 50 μm/s. Inset also shows GISAXS image of the same film. Scale bar is 200 nm. (b) Schematic of the CZA−SS process that utilizes a templated PDMS mold. (c−j) AFM images of large and small areas on the CZA−SS annealed BCP film.

peak is testament of a highly ordered BCP film well-aligned in the CZA−SS direction.

Finally, a most exciting aspect of CZA−SS is its ability to direct BCP cylinder orientation independent of external microscopic template patterns. Figure 5b shows CZA−SS where the confining topographic PDMS is a multipatterned mold rather than a smooth layer. Figure 5c−j shows the PDMS mold pattern *versus* the BCP cylinder AFM scans, illustrating how CZA−SS exerts precise control on the BCP cylinder orientation, entirely decoupled from the mold pattern's orientation, shape, and height. The time required to fill the mold is given by the equation $t_{fill} = 2\eta z^2/R\sigma' \cos\theta$ (where η is the polymer zero shear viscosity at particular temperature, z = 120 nm is the mold depth, R is the hydraulic radius ~half the trench width, σ' is the polymer surface energy at particular temperature, θ is the contact angle at the polymer−mold interface).[37] At 140 °C ($\eta \sim 10^5$ Pa·s, $\sigma' \sim 35$ mN/m, $\theta \sim 85°$), t_{fill} is less than 2 s for mold patterns with 1 μm trench widths (*i.e.*, $t_{fill} \ll$ time required for the BCP film to travel from 140 to 140 °C on the thermal gradient). Therefore, the mold-filling process does not compete with the CZA−SS process. Additionally, mold patterns are microscopic in size with width dimensions $\ll W_{peak}$, which further explains why mold pattern orientation does not interfere with BCP cylinder orientation. Technologically, this facile and independent hierarchical patterning strategy may be important to practical applications of BCPs for device manufacturing and, to our knowledge, is not achievable with any other method.

CONCLUSION

We have innovated a novel DSA method termed CZA−SS to continuously fabricate highly oriented BCP cylinders on rigid or flexible substrates at industrially relevant speeds (12 mm/min). CZA−SS is an extremely robust method that works with any T_g accessible BCP over a wide film thickness range, at the least up to 1 μm. CZA−SS is based on the unique concept of directing the differential thermal expansion between an elastomeric capping overlayer and the BCP film *via* a dynamic thermal field to induce a directional gradient shear field. The molecular mechanism responsible for cylinder orientation is the localized single oscillatory shear cycle experienced by the BCP film due to the expansion and subsequent contraction of the PDMS capping layer in the heating and cooling section of the thermal field, respectively. The maximum lateral shear stress due to this oscillatory PDMS movement occurs at the T_{MAX} on the dynamic thermal field and is an order of magnitude greater (*ca.* 12 × 10^4 Pa) than that used for mechanical soft-shear studies (*ca.* 10^4 Pa) on cylindrical BCPs.[26] We have shown two extremely simple modifications of CZA−SS that can be directly incorporated by the industry on their existing roll-to-roll

processing lines. A unique advantage of CZA-SS over other DSA methods is its ability to precisely direct BCP cylinders over microscopic patterns at any user-specified angle. Such an application has not been reported before and may open new avenues of applied research.

METHODS

Thin film samples of poly(styrene-*block*-methylmethacrylate) (PS-PMMA) and poly(styrene-*block*-2-vinylpyridine) (PS-P2VP) diblock copolymers were used in these studies. PS-PMMA, total molar mass 47.5 kg/mol (35−12.5 kg/mol, PDI ∼ 1.07) and 82 kg/mol (57−25 kg/mol, PDI ∼ 1.07), and PS-P2VP, total molar mass 34 kg/mol (23.6−10.4 kg/mol, PDI ∼ 1.04), were bought from Polymer Source Inc. and used as obtained. Sylgard-182 (Dow Corning Corp., USA) was used for making polydimethylsiloxane (PDMS) films. A mixture of PDMS elastomer/curing agent (5:1 weight ratio) was poured either on glass microscope slides or on patterned silicon templates and deaerated in vacuum. This mixture was cured at 120 °C for 6 h. PDMS was then peeled off the glass slide or patterned template to obtain 0.2−0.5 mm thick smooth or patterned films, respectively. BCP thin films were coated on ultraviolet−ozone cleaned quartz substrates (G.M. Associates, Inc.). BCP thin films were also coated on 50 μm thick polyimide films "DuPont Kapton PV 9101" (Kapton) that were provided by DuPont and used as obtained. Prior to the annealing process, samples were dried at 60 °C for 24 h under vacuum. The procedure for CZA−SS experiments is identical to the procedure for CZA−S experiments and has been explained in detail in our recent[23] paper. The sharp thermal gradient is based on the original hot-wire design concept by Lovinger *et al.*[24,38] for directional crystallization of semicrystalline polymers. Topography of these films was imaged using Dimension Icon atomic force microscopy (AFM) (Bruker AXS) in the peak force quantitative nanomechanical property mapping mode. GISAXS measurements were performed at the X9 beamline of the National Synchrotron Light Source (NSLS) at Brookhaven National Laboratory. An incident X-ray beam of 13.5 keV (wavelength = 0.0918 nm) energy was used, and samples were measured under vacuum (∼40 Pa). GISAXS experiments were performed at 0.15° incidence angle, that is, above the film−vacuum critical angle, with data collected using a charge-coupled device (CCD) detector. Data conversion to *q*-space was accomplished using silver behenate powder as a standard.

Conflict of Interest: The authors declare no competing financial interest.

Acknowledgment. We would like to thank Prof. Shi-Qing Wang (The University of Akron), Dr. Christopher Stafford (NIST, USA), Dr. Diya Bandyopadhyay (The University of Akron), Dr. Manish Kulkarni (The University of Akron), and Arvind Modi (The University of Akron) for useful discussions. This CZA−SS research work was entirely supported by the National Science Foundation (NSF), Division of Materials Research (DMR), Grant NSF DMR-1006421. Supporting GISAXS was carried out in part at the National Synchrotron Light Source, and the Center for Functional Nanomaterials, Brookhaven National Laboratory, which is supported by the U.S. Department of Energy, Office of Basic Energy Sciences, under Contract No. DE-AC02-98CH10886.

Supporting Information Available: Images showing AFM orientation analysis of CZA−SS annealed BCP film along with it is comparison with the thermally oven annealed counterpart and BCP film CZA−SS annealed on Kapton substrate. This material is available free of charge *via* the Internet at http://pubs.acs.org.

REFERENCES AND NOTES

1. Ivan, M. G.; Scaiano, J. C. *Photochemistry And Photophysics Of Polymer Materials*; Ivan, M. G., Scaiano, J. C., Eds.; John Wiley & Sons, Inc.: New York, 2010; Chapter 12.
2. Fuechsle, M.; Miwa, J. A.; Mahapatra, S.; Ryu, H.; Lee, S.; Warschkow, O.; Hollenberg, L. C. L.; Klimeck, G.; Simmons, M. Y. A Single-Atom Transistor. *Nat. Nanotechnol.* **2012**, *7*, 242–246.
3. Darling, S. B. Directing the Self Assembly of Block Copolymers. *Prog. Polym. Sci.* **2007**, *32*, 1152–1204.
4. Park, S.; Lee, D. H.; Xu, J.; Kim, B.; Hong, S. W.; Jeong, U.; Xu, T.; Russell, T. P. Macroscopic 10-Terabit-per-Square-Inch Arrays from Block Copolymers with Lateral Order. *Science* **2009**, *323*, 1030–1033.
5. Kim, S. O.; Solak, H. H.; Stoykovich, M. P.; Ferrier, N. J.; de Pablo, J. J.; Nealey, P. F. Epitaxial Self-Assembly of Block Copolymers on Lithographically Defined Nanopatterned Substrates. *Nature* **2003**, *424*, 411–414.
6. Bita, I.; Yang, J. K. W.; Jung, Y. S.; Ross, C. A.; Thomas, E. L.; Berggren, K. K. Graphoepitaxy of Self-Assembled Block Copolymers On Two-Dimensional Periodic Patterned Templates. *Science* **2008**, *321*, 939–943.
7. Tang, C.; Tracz, A.; Kruk, M.; Zhang, R.; Smilgies, D.-M.; Matyjaszewski, K.; Kowalewski, T. Long-Range Ordered Thin Films of Block Copolymers Prepared by Zone-Casting and Their Thermal Conversion into Ordered Nanostructured Carbon. *J. Am. Chem. Soc.* **2005**, *127*, 6918–6919.
8. Tang, C.; Lennon, E. M.; Fredrickson, G. H.; Kramer, E. J.; Hawker, C. J. Evolution of Block Copolymer Square Arrays. *Science* **2008**, *322*, 429–432.
9. Cheng, J. Y.; Mayes, A. M.; Ross, C. A. Nanostructure Engineering by Templated Self-Assembly of Block Copolymers. *Nat. Mater.* **2004**, *3*, 823–828.
10. Stoykovich, M. P.; Müller, M.; Kim, S. O.; Solak, H. H.; Edwards, E. W.; de Pablo, J. J.; Nealey, P. F. Directed Assembly of Block Copolymer Blends into Nonregular Device-Oriented Structures. *Science* **2005**, *308*, 1442–1446.
11. Zhao, Y.; Thorkelsson, K.; Mastroianni, A. J.; Schilling, T.; Luther, J. M.; Rancatore, B. J.; Matsunaga, K.; Jinnai, H.; Wu, Y.; Poulsen, D.; *et al.* Small-Molecule-Directed Nanoparticle Assembly towards Stimuli-Responsive Nanocomposites. *Nat. Mater.* **2009**, *8*, 979–985.
12. Peinemann, K.-V.; Abetz, V.; Simon, P. F. W. Asymmetric Superstructure Formed in a Block Copolymer *via* Phase Separation. *Nat. Mater.* **2007**, *6*, 992–996.
13. Yang, S. Y.; Yang, J.-A.; Kim, E.-S.; Jeon, G.; Oh, E. J.; Choi, K. Y.; Hahn, S. K.; Kim, J. K. Single-File Diffusion of Protein Drugs through Cylindrical Nanochannels. *ACS Nano* **2010**, *4*, 3817–3822.
14. Jung, Y. S.; Jung, W.; Tuller, H. L.; Ross, C. A. Nanowire Conductive Polymer Gas Sensor Patterned Using Self-Assembled Block Copolymer Lithography. *Nano Lett.* **2008**, *8*, 3776–3780.
15. Chai, J.; Wang, D.; Fan, X.; Buriak, J. M. Assembly of Aligned Linear Metallic Patterns On Silicon. *Nat. Nanotechnol.* **2007**, *2*, 500–506.
16. Peng, Q.; Tseng, Y.-C.; Darling, S. B.; Elam, J. W. Nanoscopic Patterned Materials with Tunable Dimensions *via* Atomic Layer Deposition on Block Copolymers. *Adv. Mater.* **2010**, *22*, 5129–5133.
17. Tseng, Y.-C.; Peng, Q.; Ocola, L. E.; Elam, J. W.; Darling, S. B. Enhanced Block Copolymer Lithography Using Sequential Infiltration Synthesis. *J. Phys. Chem. C* **2011**, *115*, 17725–17729.
18. Zhang, X.; Harris, K. D.; Wu, N. L. Y.; Murphy, J. N.; Buriak, J. M. Fast Assembly of Ordered Block Copolymer Nanostructures through Microwave Annealing. *ACS Nano* **2010**, *4*, 7021–7029.
19. Pfann, W. G. Zone Melting. *Science* **1962**, *135*, 1101–1109.
20. Bodycomb, J.; Funaki, Y.; Kimishima, K.; Hashimoto, T. Single-Grain Lamellar Microdomain from a Diblock Copolymer. *Macromolecules* **1999**, *32*, 2075–2077.

21. Angelescu, D. E.; Waller, J. H.; Adamson, D. H.; Register, R. A.; Chaikin, P. M. Enhanced Order of Block Copolymer Cylinders in Single-Layer Films Using a Sweeping Solidification Front. *Adv. Mater.* **2007**, *19*, 2687–2690.
22. Berry, B. C.; Bosse, A. W.; Douglas, J. F.; Jones, R. L.; Karim, A. Orientational Order in Block Copolymer Films Zone Annealed below the Order−Disorder Transition Temperature. *Nano Lett.* **2007**, *7*, 2789–2794.
23. Singh, G.; Yager, K. G.; Smilgies, D.-M.; Kulkarni, M. M.; Bucknall, D. G.; Karim, A. Tuning Molecular Relaxation for Vertical Orientation in Cylindrical Block Copolymer Films *via* Sharp Dynamic Zone Annealing. *Macromolecules* **2012**, *45*, 7107–7117.
24. Lovinger, A. J.; Chua, J. O.; Gryte, C. C. Studies on the α and β Forms of Isotactic Polypropylene by Crystallization in a Temperature Gradient. *J. Polym. Sci., Part B: Polym. Phys.* **1977**, *15*, 641–656.
25. Iyoda, T.; Kamata, K.; Watanabe, R.; Komura, M.; Ochiai, H. Roll-to-Roll Processable PEO-LC Block Copolymer Template Films with Normally Oriented Nanocylinder Array Structures. *Microprocesses and Nanotechnology, 2007 Digest of Papers*, **2007**, 460−461. DOI: 10.1109/IMNC.2007.4456303.
26. Angelescu, D. E.; Waller, J. H.; Adamson, D. H.; Deshpande, P.; Chou, S. Y.; Register, R. A.; Chaikin, P. M. Macroscopic Orientation of Block Copolymer Cylinders in Single-Layer Films by Shearing. *Adv. Mater.* **2004**, *16*, 1736–1740.
27. Wu, M.; Register, R. A.; Chaikin, P. Shear Alignment of Sphere-Morphology Block Copolymer Thin Films with Viscous Fluid Flow. *Phys. Rev. E* **2006**, *74*, 040801-1–040801-4.
28. Marencic, A.; Chaikin, P.; Register, R. A. Orientational Order in Cylinder-Forming Block Copolymer Thin Films. *Phys. Rev. E* **2012**, *86*, 021507−1–021507−8.
29. Hong, S. W.; Huh, J.; Gu, X.; Lee, D. H.; Jo, W. H.; Park, S.; Xu, T.; Russell, T. P. Unidirectionally Aligned Line Patterns Driven by Entropic Effects on Faceted Surfaces. *Proc. Natl. Acad. Sci. U.S.A.* **2012**, *109*, 1402–1406.
30. Hong, S. W.; Voronov, D. L.; Lee, D. H.; Hexemer, A.; Padmore, H. A.; Xu, T.; Russell, T. P. Controlled Orientation of Block Copolymers on Defect-Free Faceted Surfaces. *Adv. Mater.* **2012**, *24*, 4278–4283.
31. Mark, J. E. *Polymer Data Handbook*; Oxford University Press, Inc.: New York, 1999.
32. Tsui, O. K. C.; Russell, T. P.; Hawker, C. J. Effect of Interfacial Interactions on the Glass Transition of Polymer Thin Films. *Macromolecules* **2001**, *34*, 5535–5539.
33. Scharfenberg, S.; Rocklin, D. Z.; Chialvo, C.; Weaver, R. L.; Goldbart, P. M.; Mason, N. Probing the Mechanical Properties of Graphene Using a Corrugated Elastic Substrate. *Appl. Phy. Lett.* **2011**, *98*, 091908-1–091908-3.
34. Yager, K. G.; Fredin, N. J.; Zhang, X.; Berry, B. C.; Karim, A.; Jones, R. L. Evolution of Block-Copolymer Order through a Moving Thermal Zone. *Soft Matter* **2010**, *6*, 92–99.
35. Bates, C. M.; Pantoja, M. A. B.; Strahan, J. R.; Dean, L. M.; Mueller, B. K.; Ellison, C. J.; Nealey, P. F.; Wilson, C. G. Synthesis and Thin-Film Orientation of Poly(styrene-*block*-trimethylsilylisoprene). *J. Polym. Sci., Part A: Polym. Chem.* **2012**, 10.1002/pola.26375.
36. Park, S.; Lee, D. H.; Russell, T. P. Self-Assembly of Block Copolymers on Flexible Substrates. *Adv. Mater.* **2010**, *22*, 1882–1884.
37. Suh, K. Y.; Kim, Y. S.; Lee, H. H. Capillary Force Lithography. *Adv. Mater.* **2001**, *13*, 1386–1389.
38. Lovinger, A. J.; Chua, J. O.; Gryte, C. C. An Apparatus for *In Situ* Microscopy of Zone Solidifying Polymers. *J. Phys. E: Sci. Instrum.* **1976**, *9*, 927–929.